A Macroscopic Model of CLASP in *A. Thaliana*

Riley Wheadon, Geoffrey Wasteneys, Eric Cytrynbaum
University of British Columbia

September 8th, 2024

1 Abstract

The CLASP protein has been shown to influence cell growth by changing the arrangement of cellulose microfibrils via the orientation of microtubule arrays (MTs) on the cell membrane. Here we present a mathematical model of this phenomenon which we verify against *in vivo* observations of *A. thaliana* roots. Our model uses data from the brassinosteroid (BR) signalling pathway and predicts its downstream effects on CLASP, MTs, and ultimately root growth. Additionally, the model accurately explains the behaviour of various mutant roots in which elements of the aforementioned signalling network are edited or removed. We find that BR signalling alone is unable to predict observed rates of cell growth in the root and conclude that CLASP is essential for root zonation.

2 Background

2.1 Root Zonation

The growing root of *A. thaliana* can be roughly divided into six distinct zones, with the cells in each zone exhibiting qualitatively distinct behaviour. At the tip of the root lies the root cap, a region of cells that are constantly sluffed off to protect the growing root from debris (Kumpf and Nowack, 2015). Above the root cap is a small group of static cells known as the quiescent centre (henceforth QC), which play a crucial role in the regeneration of the root cap and surrounding cells (Matosevich and Efroni, 2021). The models presented in this paper will ignore these two regions and measure position within the root as the distance in µm from the QC.

In the meristematic zone (henceforth MZ), cells experience rapid cell division and slower cell growth. In this region, cells grow from 4.5µm to 9µm over a period of about 18h (Verbelen et al., 2006) while moving from 0µm to 200µm above the QC. Above the meristematic zone is the transition zone (henceforth TZ), in which cells experience lower rates of division and grow from 9µm to 30µm over the course of 10h (Verbelen et al., 2006). The TZ spans from approximately 200µm to 520µm above the QC. Next to the TZ is the elongation zone (henceforth EZ), where cells grow rapidly from 30µm to 130µm over the course of 4h (Verbelen et al., 2006). After leaving the EZ at approximately 900µm above the QC, cells begin differentiation and cease growth. Thus the final and most proximal region of the root is aptly named the differentiation zone (henceforth DZ).

2.2 CLASP and Microtubules

Microtubules (henceforth MTs) are tubulin polymers located on the plasma membrane of the cell which guide the deposition of cellulose on the cell wall (Hamant and Traas, 2010). When the MTs and cellulose microfibrils are deposited orthogonally to the axis of growth, the cell experiences anisotropic growth. If the MTs and cellulose are less organized, then the turgor pressure within the cell faces isotropic resistance which ultimately inhibits growth (Hamant and Traas, 2010).

The CLASP protein plays an essential role in MT patterning through its ability to help MTs cross sharp edges on the cell membrane (C. Ambrose et al., 2011). This results formation of bundles of MTs along the transverse, radial, and longitudinal edges of the cell (Halat et al., 2022). Bundles along the transverse and radial edges (henceforth TFBs), are of particular interest because they lead to microtubule arrangements that run parallel to the axis of growth. These TFBs disrupt the formation of circumferential cellulose microfibrils, which ultimately inhibits cell growth (Halat et al., 2022).

Cell length modulates the effect of CLASP on MT patterning due to the fact that longer cells have longer longitudinal edges relative to their radial and transverse edges. This causes the CLASP protein to localize towards the longitudinal edges and away from the radial and transverse edges, leading to a reduction in TFBs and an increase in growth (Halat et al., 2022). A diagram of this phenomenon from Halat et al., 2022 is shown in Figure 1.

2.3 Brassinosteroid

Brassinosteroids (BRs) are a class of plant hormones that have shown to promote both longitudinal and radial growth in a spatiotemporal manner (Ackerman-Lavert and Savaldi-Goldstein, 2020). Extracellular BRs, particularly brassinoslide (henceforth BL), bind to the BR receptor BRI1 and its homologues on the cell membrane (Vukašinović et al., 2021). This releases the inhibition of the BZR1/BES1 transcription factors by the BIN2 signalling inhibitor (Ackerman-Lavert and Savaldi-Goldstein, 2020). The effects of BR signalling have been shown to be stronger in the TZ and stronger still in the EZ due to a higher concentration of BR precursors (Vukašinović et al., 2021).

The BZR1/BES1 transcription factors, which are often used as a proxy for BR signalling, have been shown to inhibit CLASP by binding directly to its promoter and repressing its activity (Ruan et al., 2018). Additionally, CLASP influences the BR signalling network by promoting the recycling of endocytosed BRI1 receptors. Together, these two effects produce a stable postive-negative feedback loop that helps to ensure homeostasis in the root (Ruan et al., 2018).

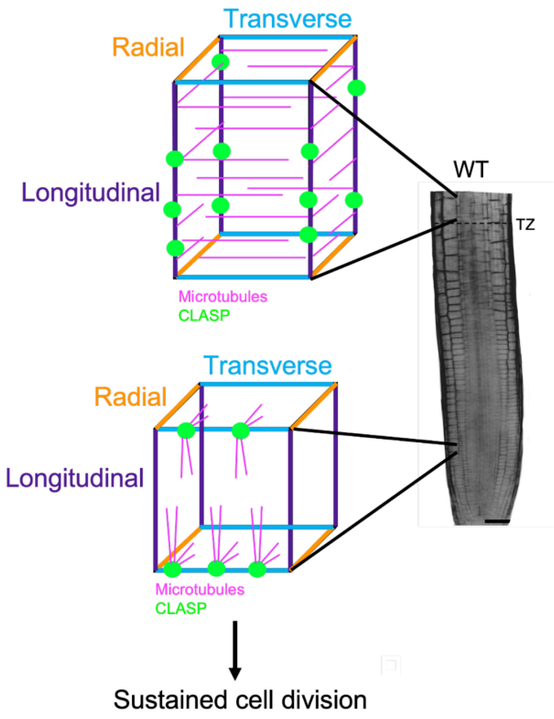

Figure 1: In longer cells, CLASP localizes to the longitudinal edges which drives a reduction in TFBs and promotes cell growth.

2.4 Mutant Roots

Making small changes to the network of proteins and hormones described in the prior two sections leads to significant changes in root phenotypes. This paper explores the *clasp-1* (J. C. Ambrose et al., 2007) *brinCLASPpro* (Ruan et al., 2018) mutant roots. The *clasp-1* root has a loss-of-function mutation that entirely inhibits the production of CLASP, which ultimately leads to an increase in cell growth through the previously discussed pathway (Halat et al., 2022). However, the rapid cell growth results in fewer cell divisions and thus fewer cells in the *clasp-1* root (Halat et al., 2022), resulting in a lower rate of overall root growth relative to the wild type (J. C. Ambrose et al., 2007).

In wild type roots, the transcription of the CLASP protein is inhibited whenthe root is exposed to exogenous BRs (Ruan et al., 2018). However, the *brinCLASPpro* root is insensitive to the effects of BR signalling, meaning the application of exogenous BRs does not affect the amount of CLASP in this mutant. It therefore stands to reason that the *brinCLASPpro* mutant should have more CLASP than the wild type due to the abscence of this inhibition. It has been shown that an excess of CLASP upregulates the level of BR signalling by promoting the recycling of BRI1 receptors (Ruan et al., 2018), and we speculate that this leads to the increased cell growth observed in *brinCLASPpro* mutants relative to the wild type. A plot of cell size across the mutants and the wild type is shown in Figure 2.

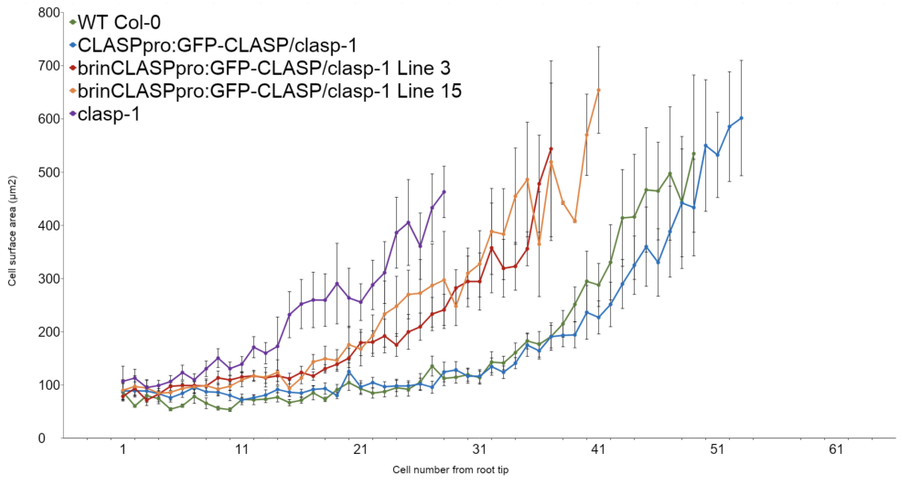

Figure 2: Average cell areas plotted against cell number for each of the two mutant roots and the wild type. This data was taken from trichoblast cell columns in the epidermis. The GFP-CLASP line drives the expression of a fluorescent fusion protein which fully complements the *clasp-1* mutant (C. Ambrose et al., 2011). Therefore, the GFP-CLASP/clasp-1 root is phenotypically similar to the wild type. Observe that the *clasp-1* mutant has the largest cells, followed by the *brinCLASPpro* mutant, followed by the wild type.

3 Model

3.1 Brassinoslide Component

Vukašinović et al., 2021 provide a detailed biosynthetic pathway for BL, which is presented in Figure 3. Since BL is the most biochemically active brassinosteroid van Esse et al., 2012, we will assume that it is only brassinosteroid when modelling.

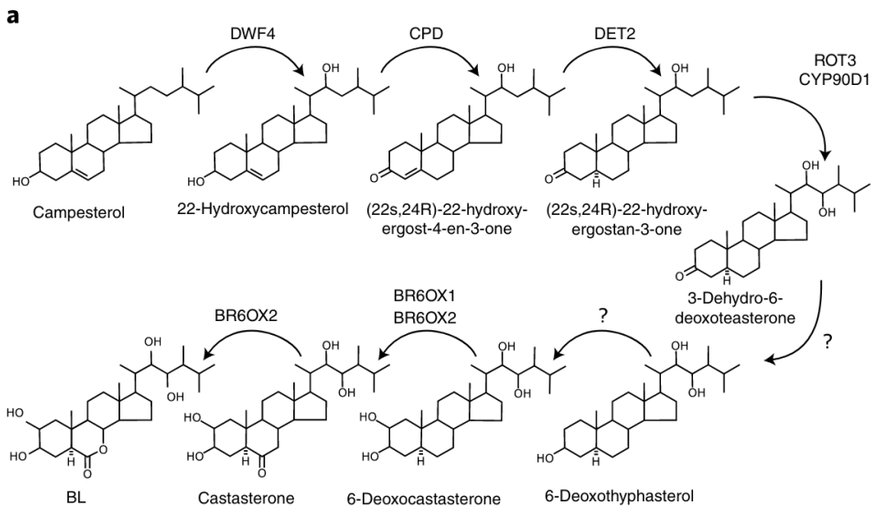

Figure 3: Biosynthetic pathway leading to the formation of BL from campesterol. Mutants deficient in each of the enzymes shown above the transition arrows (DWF4, CPD, DET2, etc.) exhibited stunted growth (Vukašinović et al., 2021).

The biosynthetic enzymes CPD and ROT3 were observed by Vukašinović et al., 2021 using fluorescence imaging in the vascular cell columns of a single root. Their results are shown in Figure 4.

We make the assumption that the fluorescence intensity of CPD and ROT3 correspond to the concentration of BL ligand up to some scalar multiple. To determine this scalar, we use an estimate from van Esse et al., 2012 that gives the extracellular concentration of BL ligand to be at most $1\text{nmol}\,\text{L}^{-1}$in wild-type roots. This gives us the following formula for the extracellular BL concentration [BL] in $\text{nmol}\,\text{L}^{-1}$:

$$[\text{BL}] = b \cdot \frac{\text{CPD}}{\max(\text{CPD})} + (1-b) \cdot \frac{\text{ROT3}}{\max(\text{ROT3})} \tag{1}$$

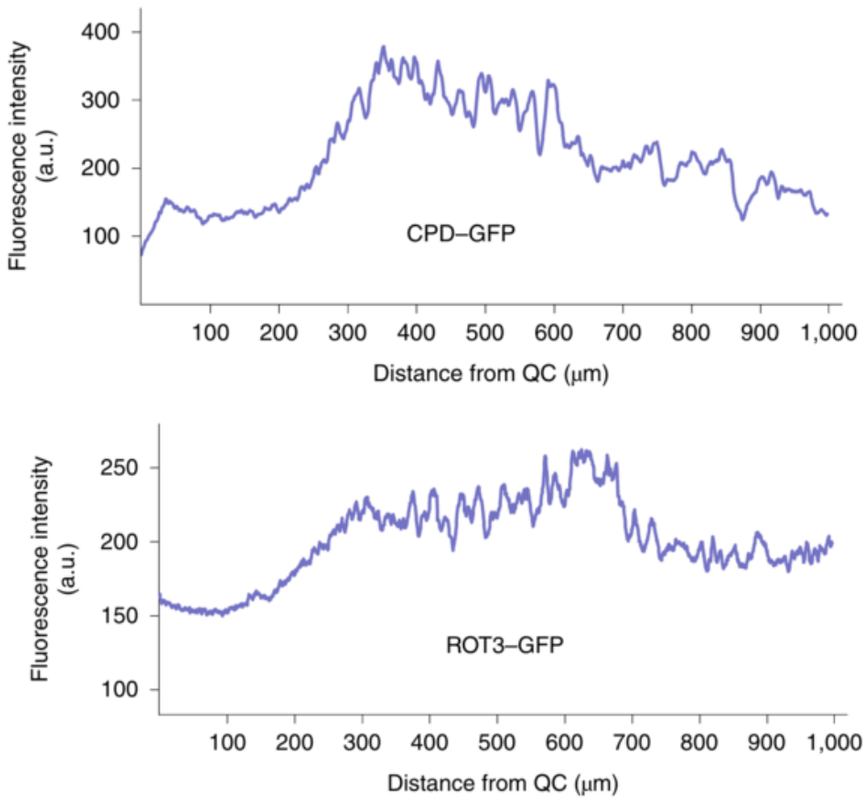

Figure 4: The levels of CPD and ROT3 remain relatively constant in the meristem (0-200µm) before increasing in the transition zone (200-400µm) and reaching a maximum in the elongation zone (400-700µm) (Vukašinović et al., 2021).

In (1), the parameter $b \in [0, 1]$ controls the bias towards CPD in order to account for the fact that the exact details of the BL pathway are omitted from our model. Using the data from Figure 4 along with (1), we get the plot of BL concentration against position shown in Figure 5.

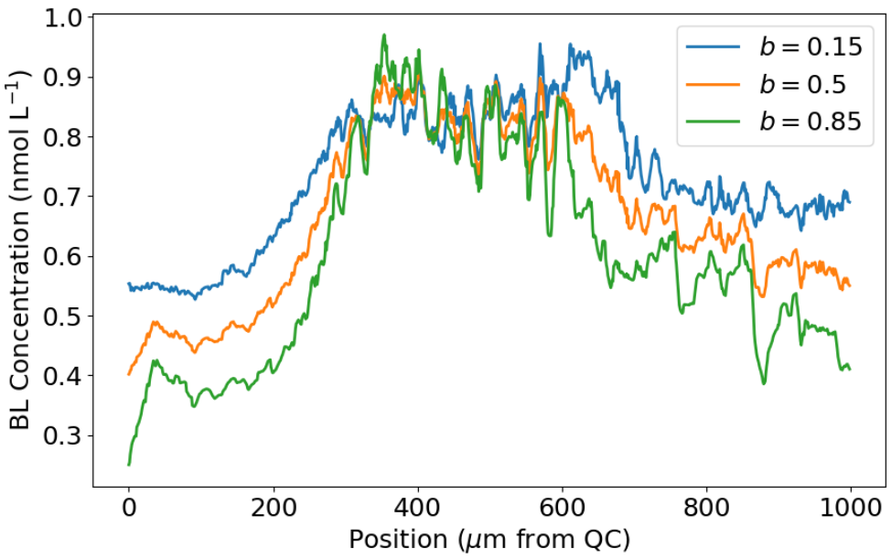

Figure 5: The BL concentration function for three different values of the bias parameter b. For future simulations we will use $b = 0.5$, since the BL concentration function exhibits similar qualitative behaviour for all b as shown above.

Additionally, BR biosynthetic enzymes have been shown to move short distances in the root (Vukašinović et al., 2021), so we take an n µm moving average of the BL concentration function to account for diffusion. Shown in Figure 6 is a plot of the BL concentration function after the moving average has been applied to the CPD and ROT3 functions.

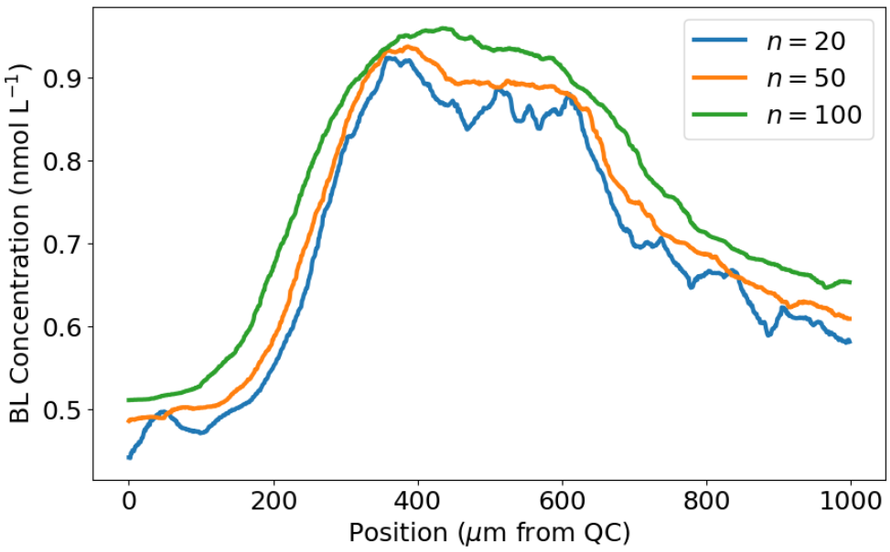

Figure 6: A plot of BL concentration functions ($b = 0.5$) for three different values of the moving average period n. Future simulations will use $n = 50$, an admittedly arbitrary choice since the exact details of the diffusive effect we are modelling are unknown.

3.2 BRI1 Receptor Component

From the description of the BL concentration function in Equation (1) we can derive a formula for the concentration of bound BRI1 receptors at any position in the root. To do this, we use the equilibrium and mass-balance equations for the BRI1 receptor network introduced by van Esse et al., 2012.

$$[\text{BRI1 BL}] = \frac{[\text{BRI1}_{\text{free}}] \cdot [\text{BL}_{\text{free}}]}{K_d} \tag{2}$$

$$\begin{aligned} [\text{BRI1}] &= [\text{BRI1 BL}] + [\text{BRI1}_{\text{free}}] \\ [\text{BL}] &= [\text{BRI1 BL}] + [\text{BL}_{\text{free}}] \end{aligned} \tag{3}$$

In the equations above, [BRI1 BL] denotes the concentration of bound BRI1 receptors, which are assumed to bind at a ratio of one molecule to one monomer (van Esse et al., 2012). K_d is the BL dissociation constant. Additionally, [BRI1$_{\text{free}}$] and [BL$_{\text{free}}$] denote the unbound BRI1 and BL concentrations respectively, while [BL] and [BRI1] represent the total BRI1 and BL concentrations. To further simplify our model, we can express [BRI1 BL] as a function of [BRI1] and [BL] by substituting (3) into (2) to get:

$$[\text{BRI1 BL}] = \frac{([\text{BRI1}] - [\text{BRI1 BL}])([\text{BL}] - [\text{BRI1 BL}])}{K_d} \tag{4}$$

$$K_d \cdot [\text{BRI1 BL}] = [\text{BRI1}] \cdot [\text{BL}] - ([\text{BL}] + [\text{BRI1}]) \cdot [\text{BRI1 BL}] + [\text{BRI1 BL}]^2 \tag{5}$$

$$[\text{BRI1 BL}]^2 - ([\text{BL}] + [\text{BRI1}] + K_d) \cdot [\text{BRI1 BL}] + ([\text{BRI1}] \cdot [\text{BL}]) = 0 \tag{6}$$

Now, we can use the quadratic formula to determine the positive value of [BRI1 BL] for which (6) holds. This gives us a formula for [BRI1 BL] in terms of [BRI1] and [BR], where $A = ([\text{BL}] + [\text{BRI1}] + K_d)$.

$$[\text{BRI1 BL}] = \frac{A - \sqrt{A^2 - 4 \cdot [\text{BRI1}] \cdot [\text{BL}]}}{2} \tag{7}$$

Empirical research gives us estimates for the values of [BRI1] and K_d. van Esse et al., 2012 estimate the BRI1 receptor concentration to be $62 \pm 4\text{nmol L}^{-1}$ in wild type roots. Values for the BL dissociation constant K_d range from 7.4nmol L^{-1} to 15nmol L^{-1} (Wang et al., 2001) up to 55nmol L^{-1} (Caño-Delgado et al., 2004). For the models presented in the forthcoming sections, we will take [BRI1] $= 62\text{nmol L}^{-1}$

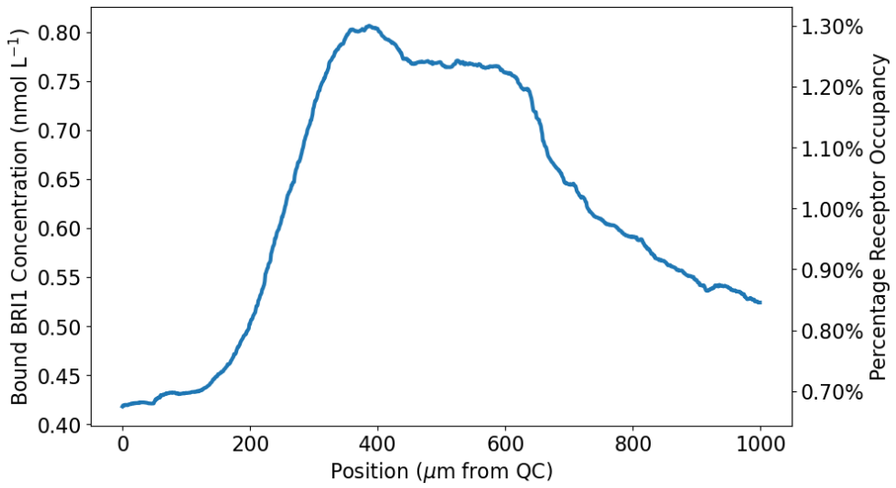

Figure 7: Plot of bound receptor concentration (left axis) measured in nmol L^{-1} as well as receptor occupancy percentage (right axis). Due to the fact that [BL] $\ll$ [BRI1] the [BRI1 BL] function is approximately equal to the [BL] function up to some scalar multiple.

and $K_d = 10\text{nmol}\,\mathrm{L}^{-1}$. Using these parameters along with the formula in equation (7) we get the [BRI1 BL] function shown in Figure 7.

Our model makes the assumption that all BRI1 receptors are localized to the cell membrane. Additionally, it assumes that the law of mass action is a reasonable approximation for the diffusing BL ligand binding to the static BRI1 receptors. We believe this decision is justified due to the low percentage occupancy of the BRI1 receptors, which suggests that any free BL ligand will have many oppourtunities to bind to a receptor. Further modelling of the BRI1 receptor network using the physical properties of the system would help to clarify and refine these assumptions.

3.3 BES1 Signalling Model

In this model and all subsequent models we aim to predict the behaviour of a single cell as it is pushed away from the quiescent centre (henceforth QC) by the growth and division of the cells beneath it. Within the meristematic zone, cells grow from a length of 4.5µm to 9µm over a period of approximately 18h (Verbelen et al., 2006). However, cells may undergo one or more divisions during this time (Goh et al., 2023), so tracking the exact lineage of a single cell is difficult. For this reason, our model will only consider cells at 150µm or higher above the QC.

Prior to writing down a system of differential equations for our model, we need to rescale our data to be in terms of time instead of position. To do this, we map a position of 150µm above the QC to $t = 0$h and then use cell lineage data from Goh et al., 2023 to determine a function that maps positions to times. The resulting position function is shown in Figure 8.

Our first model aims to predict the level of BR signalling within the cell as it moves away from the QC, measured in terms of the BES1 transcription factor. To do this, we will use a time-rescaled version of the BL concentration function shown in Figures 5 and 6 with $b = 0.5$ and $n = 50$. The model will be fit to time-rescaled fluorescence intensity data from the cell columns of a single *A. thaliana* root (Vukašinović et al., 2021). The BL concentration function and the data are shown in Figure 9. It is important to note that there is likely additional plant-to-plant variance that remains unaccounted for due to the fact that the data comes from a single organism.

With our data prepared, we can now define an ODE model for the amount of BES1 transcript in terms of the BL concentration $B(t) = [\text{BL}]$. To do this, recall that Equation (7) gives us the concentration of bound BRI1 receptors $R_B = [\text{BRI1 BL}]$ in terms of $B(t)$, the dissociation constant K_d, and the total BRI1 concentration $R_T = [\text{BRI1}]$. For this model, we will fix $K_d = 10\text{nmol}\,\mathrm{L}^{-1}$ (Wang et al., 2001) and $R_T = 62\text{nmol}\,\mathrm{L}^{-1}$ (van Esse et al., 2012) as in Figure 7.

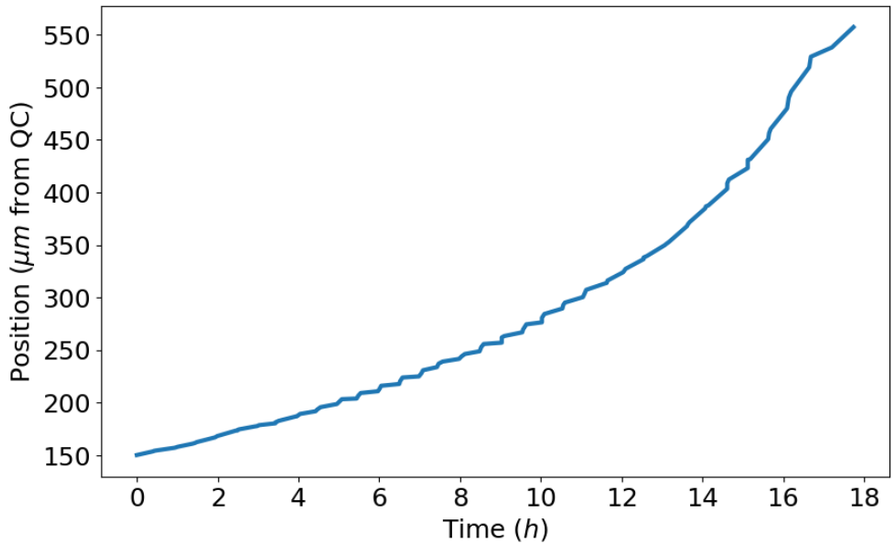

Figure 8: Plot of cell position (in µm) versus time (in h) using cell lineage data from Goh et al., 2023. The function is scaled such that $t = 0$h corresponds to a position of 150µm above the QC.

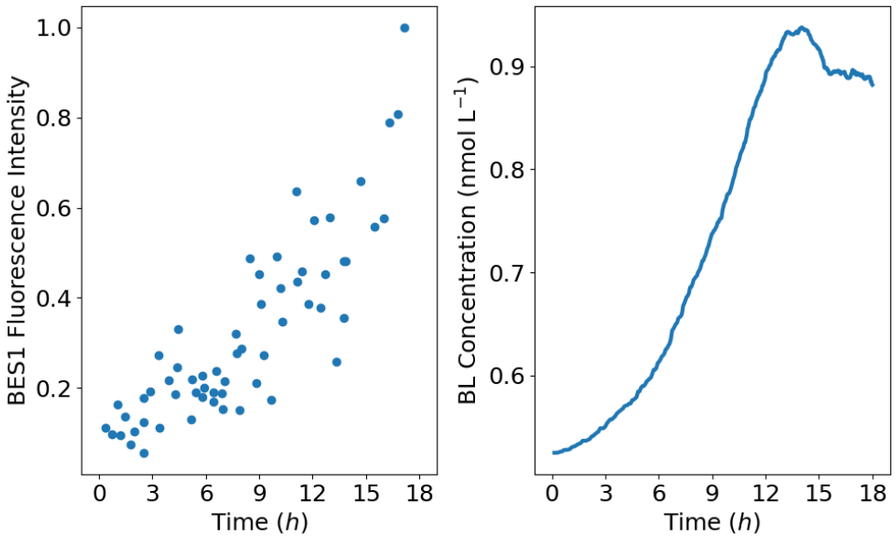

Figure 9: Plot of the transformed BES1 signalling data from Vukašinović et al., 2021 (left) and transformed BL concentration function (right). Since fluorescence intensity data is measured in arbitrary units, the BES1 plot was rescaled to a maximum value of 1.

$$R_B(B, R_T, K_d) = \frac{(B + R_T + K_d) - \sqrt{(B + R_T + K_d)^2 - 4 \cdot R_T \cdot B}}{2} \tag{8}$$

When the concentration of bound BRI1 receptors R_B is higher, the effects of the BIN2 signalling inhibitor are released, leading to increased production of BES1. Let s_{in} denote the rate at which R_B increases BES1 transcription. We also include a decay term with parameter s_{out} to account for the degradation of the BES1 transcription factor over time. The intial condition is given by another parameter $\text{BES1}(0) = s_0$. Fitting this parameter will give us a non-dimensional estimate for the level of BES1 signalling at 150µm above the QC.

$$\frac{d\text{BES1}}{dt} = s_{\text{in}} R_B(B, R_T, K_d) - s_{\text{out}}\text{BES1}, \quad \text{BES1}(0) = s_0 \tag{9}$$

Since R_B has t-dependence through the BL concentration function B, Equation (9) cannot be solved analytically and must be approximated using numerical methods. Before we show the results of these simulations, we present a visual summary of the model in Figure 10.

The BES1 function was approximated using a forward euler method with a time step of 0.01h. We evaluated the model using the Root-Mean-Squared Error

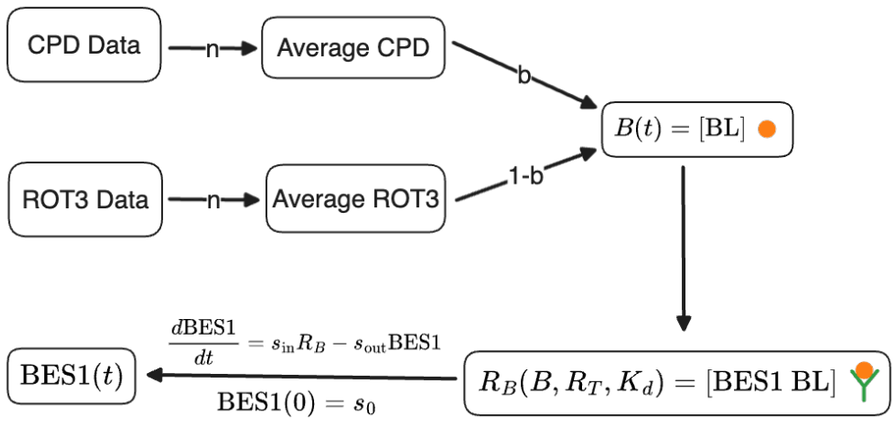

Figure 10: A visual depiction of the model up to this point. The extracellular BL concentration function $B(t)$ is computed using a moving biased average of the CPD and ROT3 biosynthetic enzymes. Then, $B(t)$ is used to determine the concentration of bound receptors R_B, building on the work of van Esse et al., 2012. Finally, an ordinary differential equation model is used to express the BES1 transcription factor as a function of time through R_B.

(RMSE) metric. The formula is given in Equation (10) where N denotes the number of observations. Each y_i $(1 \leq i \leq N)$ represents an observed value while each $f(t_i)$ denotes the model output at time t_i.

$$\mathrm{RMSE} = \sqrt{\frac{1}{N}\sum_{i=1}^{N}(y_i - f(t_i))^2} \tag{10}$$

The `scipy.optimize.minimize` function from the scientific computation package scipy was used to determine the values of $s_0 \in [0, 0.5]$, $s_{\mathrm{in}} \in [0, 0.5]$, and $s_{\mathrm{out}} \in [0, 0.5]$ that yielded the lowest error. Searching a larger parameter space did not produce a better fit (not shown). Figure 11 compares the fitted model to the experimental data.

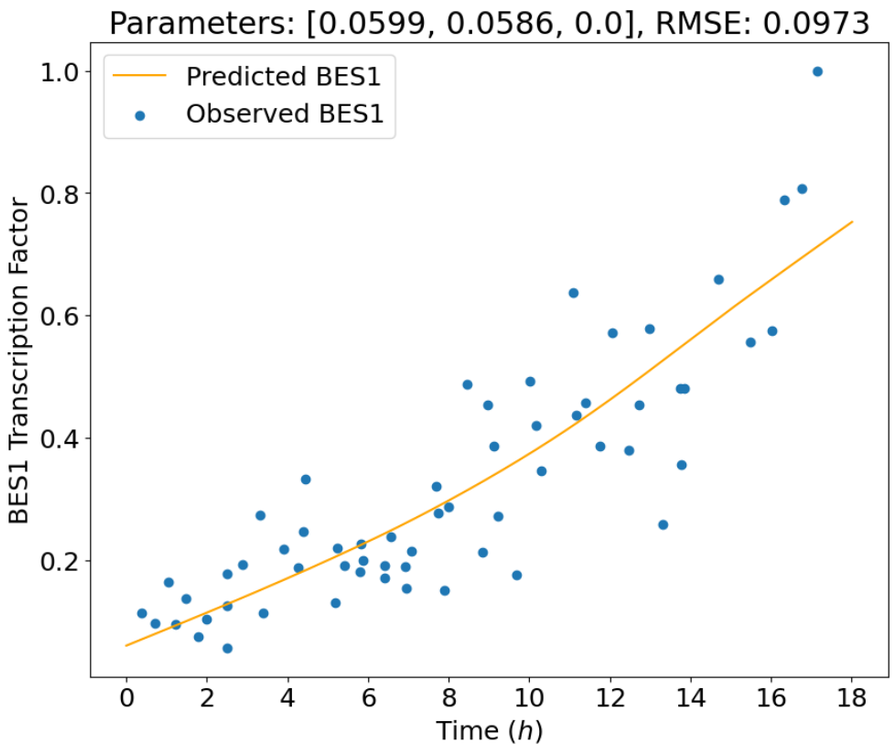

Figure 11: Results of model fitting to the BES1 signalling data from Vukašinović et al., 2021. The optimal parameter values were $s_0 = 0.0599\,\mathrm{BES1}$, $s_{\mathrm{in}} = 0.0586\,\mathrm{BES1}/R_B\mathrm{h}$ and $s_{\mathrm{out}} = 0\,\mathrm{h}^{-1}$. While s_0 and s_{in} appear accurate in the biological context of the problem, it is unlikely that $s_{\mathrm{out}} = 0$, as this suggests that the BES1 transcription factor does not decay.

Since the result $s_{\text{out}} = 0$ is not biologically accurate, we performed a search of the parameter space $(s_0, s_{\text{in}}, s_{\text{out}}) = (0.0599, x, y)$ where $0 \leq x \leq 0.5$ and $0 \leq y \leq 0.5$ to get a better idea of the model's behaviour. This will also help us quantify the sensitivity of our model to small perturbations in the parameters. To do this we divided the $s_{\text{in}} \in [0, 0.5]$ and $s_{\text{out}} \in [0, 0.5]$ domain into 100 evenly spaced points and took the cartesian product to produce a lattice of 10 000 points in parameter space. Then, we ran the model at each of these points and plotted in the error in Figure 12.

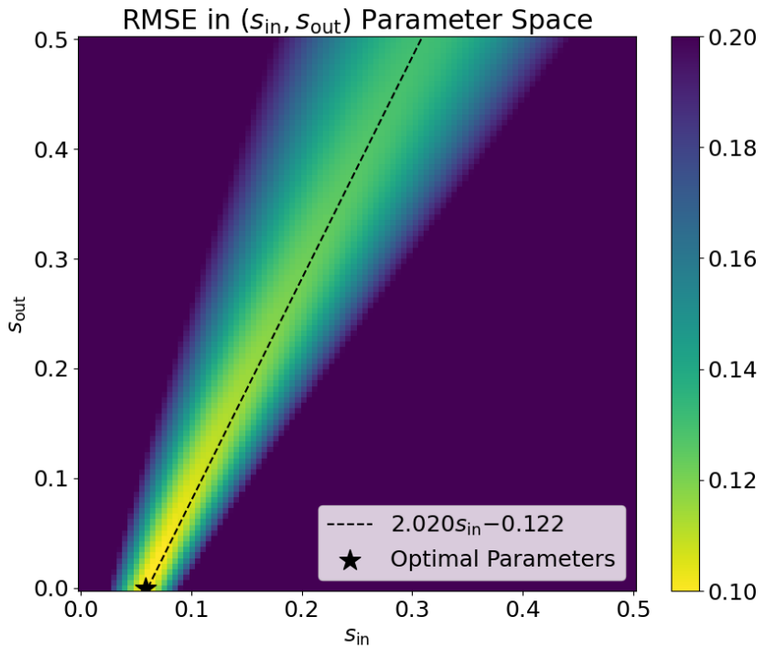

Figure 12: Heatmap showing the model RMSE for a 100×100 grid of $(s_{\text{in}}, s_{\text{out}})$ parameter values. The initial condition s_0 was fixed to its fitted value 0.0599. Regions of the plot shaded dark purple were truncated to an RMSE of 0.2 and thus the actual RMSE at these points may be higher. The results of this process indicate a clear linear relationship between s_{in} and s_{out} which is given approximately by the linear function function $s_{\text{out}} = L(s_{\text{in}}) = 2.02s_{\text{in}} - 0.122$.

The results of the parameter space search shown in Figure 12 indicate that if s_{in} or s_{out} can be determined through experiments, the other parameter value can also be estimated to a high degree of accuracy using the linear relationship $s_{\text{out}} = L(s_{\text{in}}) = 2.02s_{\text{in}} - 0.122$. This result is singificnat because it may be experimentally feasible to find s_{out}, the BES1 transcription factor decay constant, and use it to determine s_{in}, which would be difficult to determine experimentally. However, there are some caveats to this approach. Since the data has arbitrary units, quantifying s_{in} would also require making exact measurements of the BES1 transcription factor and using them to rescale Equation (9) prior to using the linear relationship we identified. Additionally, there is some uncertainty in the behaviour of the BL concentration function $B(t)$ as the exact details of the BL biosynthetic pathway were left out of the model. That being said, the scale scale of the BL concentration ($\approx 1\text{nmol}\,\text{L}^{-1}$) is grounded in the literature (van Esse et al., 2012).

The results of model fitting suggest that smaller values of s_{out} along the to $L(s_{\text{in}})$ function produce better fits. This is indicated by the brighter yellow colour near the bottom of the dotted black line in Figure 12. In the regime where s_{out} is small Equation (9) can be approximated as follows:

$$\frac{\text{BES1}}{dt} = s_{\text{in}} R_B - s_{\text{out}}\text{BES1} \approx s_{\text{in}} R_B \Rightarrow \text{BES1} \approx s_{\text{in}} \int R_B \, dt \tag{11}$$

This approximation indicates that the BES1 transcription factor accumulates over time in the cell and does not reach the maximum steady state value imposed by s_{out}. While it is unlikely that the maximum steady state value is infinite, which is implied by the fitted parameter $s_{\text{out}} = 0$, we speculate that the the true value of s_{out} is relatively small. For the sake of comparison, let us also consider the region of

our parameter space where s_{out} is large, which produces a less accurate fit. Under this regime we have the following approximation for the BES1 function:

$$\text{BES1} = \frac{s_{\text{in}} R_B}{s_{\text{out}}} + \left(s_0 - \frac{s_{\text{in}} R_B}{s_{\text{out}}} \right) e^{-s_{\text{out}} \text{BES1}} \approx \frac{s_{\text{in}} R_B}{s_{\text{out}}}$$

When s_{out} is large, the BES1 transcription factor rapidly reaches its steady state value, and is thus approximately proportional to R_B over the domain. As mentioned previously, the actual system probably does not behaves this way since the model fits poorly to the data for larger values of s_{out}.

3.4 CLASP and Cell Growth Model

The data presented in Figure 2 along with similar data for atrichoblast cells was transformed into units of time and length using the following procedure. First, we make the assumption that cells are perfect cylinders, so that their surface area is related to their length by following formula:

$$\frac{A - 2\pi r^2}{2\pi r} = L$$

Then, we assume that the radius of each cell is identical, and prescribe a suitably chosen r based on experimental data (Goh et al., 2023). To convert cell number to position we take the cumulative sum of the cell lengths over each cell column. Missing data was filled in using the average length for that cell number. Finally, we use the the function shown in Figure 8 to transform the position series into a time series and plot it against the cell lengths. The results of this data preprocessing is shown in Figures 13 and 14 for trichoblast and atrichoblast cells respectively.

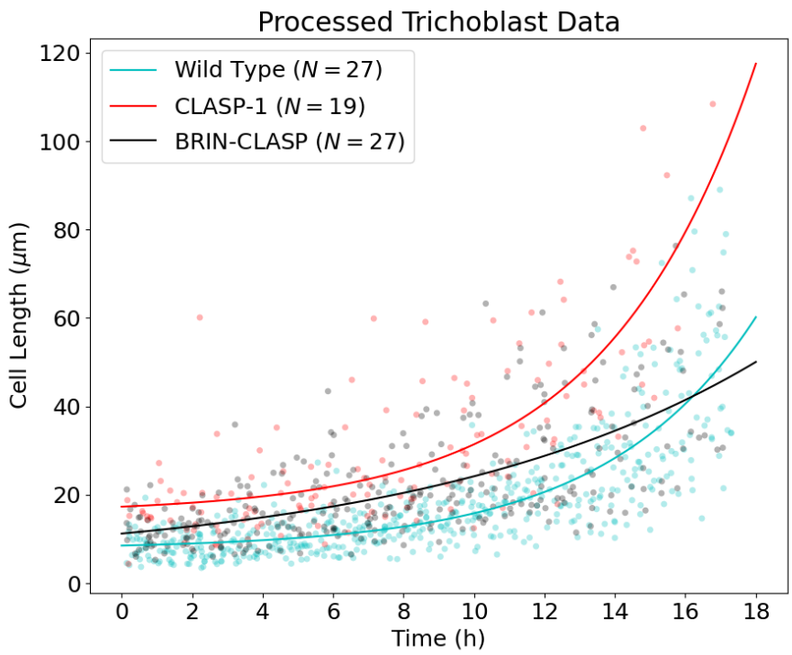

Figure 13: Plot of cell lengths from N Wild Type, CLASP-1, and BRIN-CLASP roots. The line of best fit is an exponential function of the form $A + Be^{Cx}$. Wild Type cells are on average the shortest, followed closely by BRIN-CLASP. CLASP-1 cells are significantly longer, especially in the proximal regions of the root.

For our first model of cell growth, we will consider exclusively wild type trichoblast cells. This model uses the ODE given in Equation (12), which is a variation on the model presented in Lockhart, 1965 that accounts for the promotion of cell elongation by the BES1 transcription factor (Vukašinović et al., 2021, Ackerman-Lavert and Savaldi-Goldstein, 2020).

$$\frac{dL}{dt} = (g_P + g_B \text{BES1}) L \tag{12}$$

In this model, g_P denotes the basal growth rate due to the internal turgor pressure of the cell while g_B denotes the rate at which BES1 promotes cell elongation.

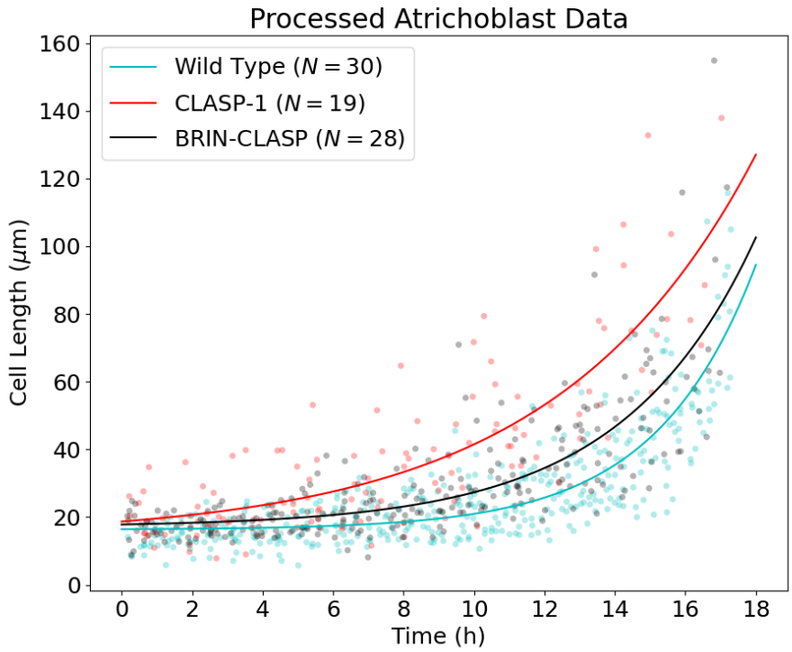

Figure 14: Plot of cell lengths from N Wild Type, CLASP-1, and BRIN-CLASP roots. The line of best fit is an exponential function of the form $A + Be^{Cx}$. Atrichoblast cells exhibit similar behaviour to trichoblast cells accross mutants, although atrichoblast cells are about 25% longer.

$\frac{dL}{dt}$ is scaled by the length L because longer cells have more locations for the cellulose to stretch and reassemble (Smithers et al., 2024). An parameter corresponding to the initial condition $L(0) = g_0$ was also fitted. This parameter represents the average cell length at 150µm above the QC.

The BES1 equation (9) and length equation (12) were approximated using a forward euler method with time step 0.01h^{-1}. Model fitting used the RMSE metric defined in equation (10) to fit the output to the data shown in Figure 13. To reduce the dimensionality of the parameter space the parameters s_0, s_{in}, and s_{out} from equation (9) were assigned their fitted values as shown in Figure 11. The parameter bounds used were $g_0 \in [0, 10]$ and $g_P, g_B \in [0, 1]$. The results of the simulation are depicted in Figure 15.

The result shown in Figure 15 suggests that our simple model is able to capture the trend in the data without invoking the existence of the CLASP protein. That being said, the abscence of the basal growth rate g_P suggests that the optimal parameter values we found may not be representative of their true values. To get a better idea of the behaviour of our model we began by performing an uncertainty analysis. To do this, we took each error $e_i = |f(t_i) - y_i|$, and then normalized it to get the percentage error $\tilde{e_i} = e_i/y_i$. Then, we took the vectors of errors $\mathbf{e}$ and computed 1000 random permutations $\mathbf{e}_1, \ldots, \mathbf{e}_{1000}$. Finally, we constructed new 1000 new data vectors $\mathbf{y}_j = f(\mathbf{t}) + \mathbf{e}_j$ and fitted the model to each one. The results of this analysis are shown in Figure 16.

A local sensitivity analysis over the domain $g_P \in [0, 0.1]$ and $g_B \in [0.1, 0.3]$ was also performed using the same methodologies described in Section 3.3. The results of this analysis are shown in Figure 17.

3.5 Mutant Models

In our final model, we introduce the CLASP protein in order to differentiate the wild type root from the CLASP-1 and BRIN-CLASP mutants. We assume that the CLASP protein C is produced at a basal rate c_{in}. As discussed previously, the BES1 transcription factor inhibits CLASP by repressing its promoter (Ruan et al., 2018, so we include a parameter c_B that represents this effect. We also include a background degradation rate c_{out}. Since C will not be fitted to experimental data and is thus dimensionless, we will assign an initial condition of $C(0) = 1$. The differential equation defining the CLASP protein is shown in equation (13).

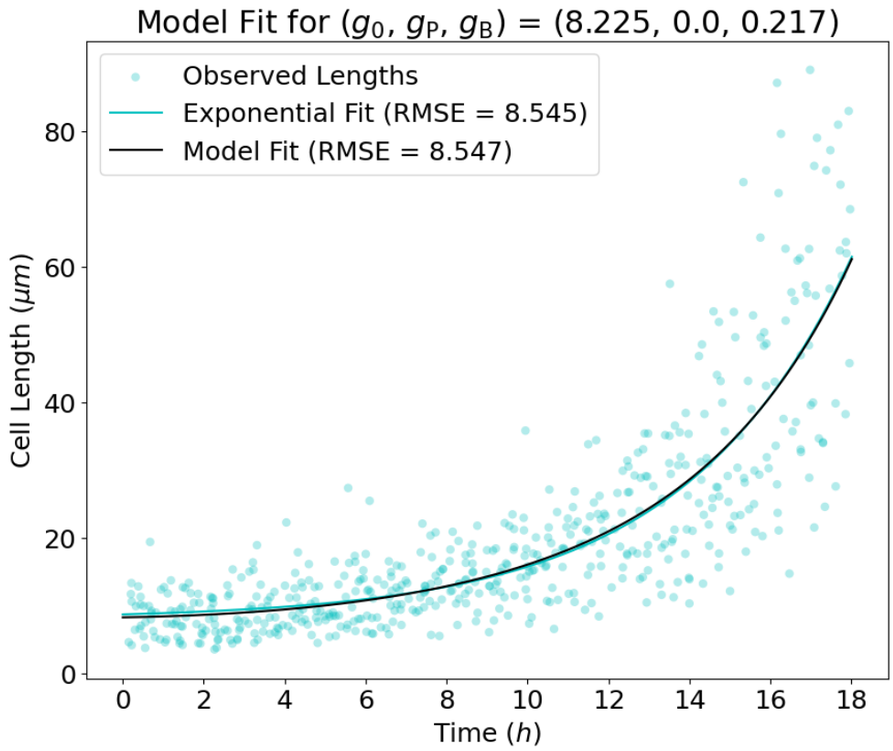

Figure 15: Results of fitting the growth model in equation (12) to cell length data. The optimal parameter values were $g_0 = 8.225\mu\text{m}$, $g_P = 0\text{h}^{-1}$ and $g_B = 0.0217\,\text{BES1}^{-1}\text{h}^{-1}$. An exponential curve of the form $A + Be^{Cx}$ was also fitted to the data as a point of comparison.

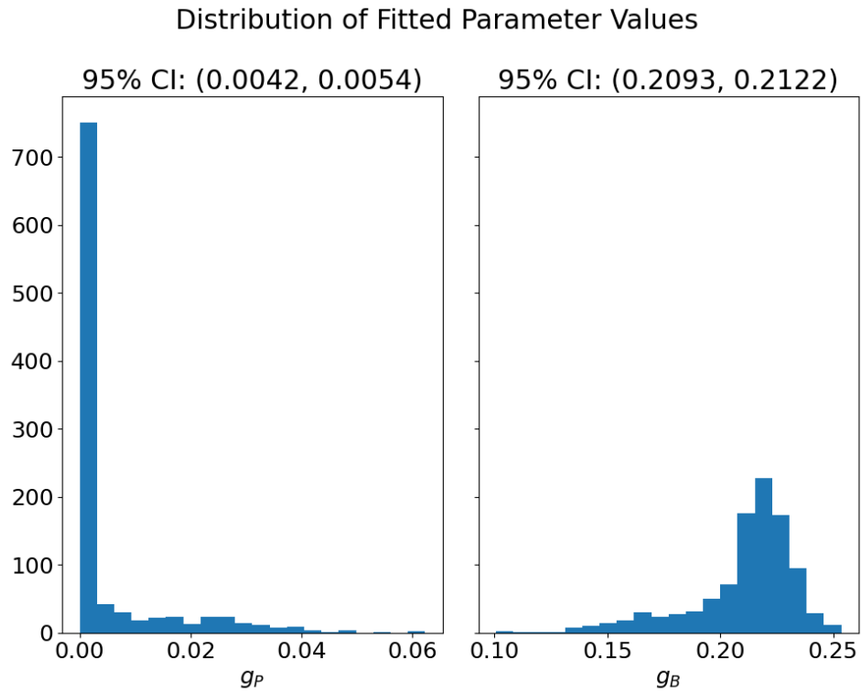

Figure 16: A plot of the distribution of fitted g_P and g_B parameter values after the error shuffling process was repeated 1000 times. Interestingly, the optimal parameters for the original data are outside the 95% confidence intervals shown above.

$$\frac{dC}{dt} = c_{\text{in}} - (c_{\text{out}} + c_B\text{BES1})C \tag{13}$$

We also need to integrate the two downstream effects of CLASP into our model. It is known that CLASP increases the concentration of BRI1 receptors by promoting their recycling (Ruan et al., 2018). Therefore, we replace the parameter [BRI1], which was previously fixed to $62\text{nmol}\,\text{L}^{-1}$, with equation (14). In this equation, r_C represents the rate at which CLASP promotes the recycling of [BRI1] receptors

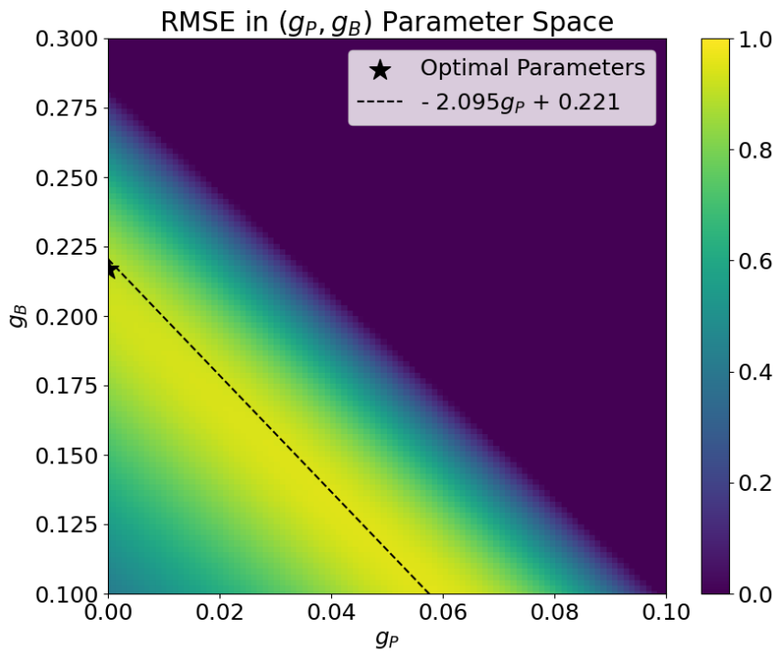

Figure 17: A heatmap of model error near the optimal parameter values $g_P = 0$ and $g_B = 0.217$. The RMSE remains low for values of g_B and g_P near the optimal range $g_B = -2.095g_P + 0.221$ but grows rapidly outside of that band. This result is not surprising given since if g_B and g_P are both high the model will overestimate the cell lengths.

while r_P denotes the basal receptor level in the abscence of CLASP.

$$[\text{BRI1}] = R_T = r_C C + r_P \tag{14}$$

Experiments have also found that CLASP inhibits growth in a length-dependent manner. Therefore, we add a $g_C C/L$ term to the denominator of equation (12) to get the modified version shown in equation (15). We also omit the g_P parameter used in equation (12) because this parameter was fit to effectively 0 in Figure 15.

$$\frac{dL}{dt} = \frac{g_B \text{BES1}}{1 + (g_C C/L)} \tag{15}$$

An overview of the entire model incorporating BL, BRI1, BES1, CLASP, and cell growth is presented in Figure 18. The differential equations used in the model were approximated using a forward euler method with time step 0.01h. The model accuracy was quantified using the sum of the RMSE from each dataset (Wild Type, CLASP-1, BRIN-CLASP). In CLASP-1 roots we fixed the parameter values $c_{\text{in}} = c_{\text{out}} = c_B = 0$. For the BRIN-CLASP root we set $c_B = 0$. All other parameters were held constant accross the three mutants.

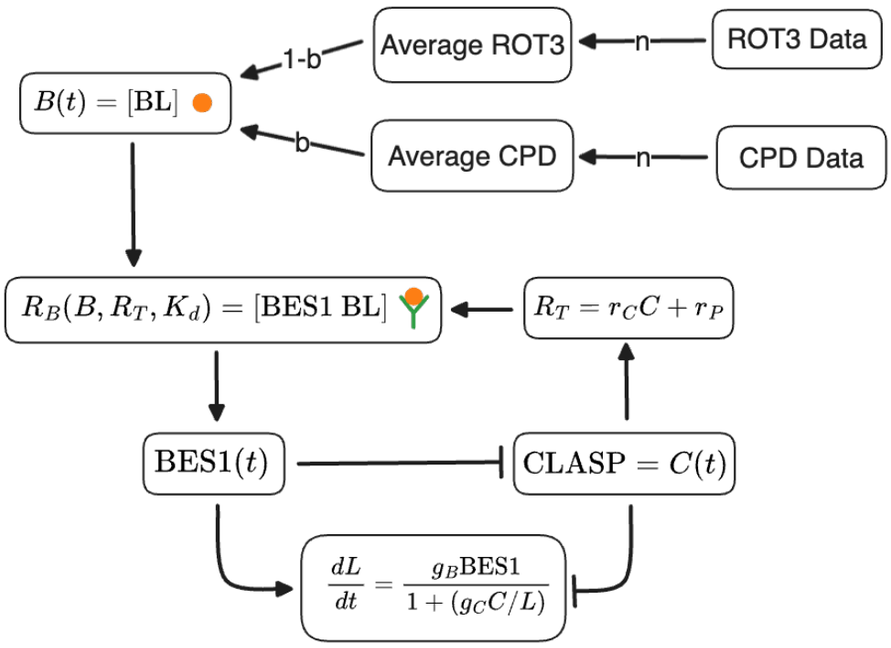

Figure 18: Our complete model of cell growth in *A. thaliana* which contains the BL concentration B, the BRI1 concentration R_T, the bound receptor concentration R_B, the level of BES1 signalling, the quantity of CLASP protein C, and the length of the cell L.

4 Discussion

Many of the parameters presented were prescribed or assigned prior to fitting the model. Some of these parameters, such as K_d (the BL dissociation constant) and R_T (the total concentration of BRI1 receptors) were based on previous results in the literature. However, other parameters such as n (the BL moving average period) and b (the CPD/ROT3 bias) were prescribed with minimal justification. This was necessary due to the fact that the data available was only able to support a small number of parameters without running the risk of overfitting. In light of new data, it may be possible to get estimates and confidence intervals for the assigned parameters.

Further experiments are necessary to more accurately fit the model. In particular, quantitative measurements of extracellular BR concentrations, CLASP protein levels, and the BES1 transcription factor would lead to significant improvements in model efficacy. The work in this paper also presents interesting oppourtunities for further modelling. Adding a model of cell division to the system of ODEs presented here would make it possible to describe an entire column of trichoblast or atrichoblast cells. This cell column model could be integrated into a two-dimensional cross section model (Grieneisen et al., 2007, Di Mambro et al., 2017, Salvi et al., 2020), which often omit the effects of BR and CLASP on growth and division. This would make it possible to study the crosstalk between BR and auxin (Chaiwanon and Wang, 2015, Vragović et al., 2015) *in silico* to help us better understand how these crucial plant hormones interact with one another.

References

Lockhart, J. A. (1965). An analysis of irreversible plant cell elongation. *Journal of Theoretical Biology*, *8*(2), 264–275. https://doi.org/10.1016/0022-5193(65)90077-9

Wang, Z.-Y., Seto, H., Fujioka, S., Yoshida, S., & Chory, J. (2001). BRI1 is a critical component of a plasma-membrane receptor for plant steroids. *Nature*, *410*(6826), 380–383. https://doi.org/10.1038/35066597

Caño-Delgado, A., Yin, Y., Yu, C., Vafeados, D., Mora-García, S., Cheng, J.-C., Nam, K. H., Li, J., & Chory, J. (2004). BRL1 and BRL3 are novel brassinosteroid receptors that function in vascular differentiation in Arabidopsis. *Development (Cambridge, England)*, *131*(21), 5341–5351. https://doi.org/10.1242/dev.01403

Verbelen, J.-P., Cnodder, T. D., Le, J., Vissenberg, K., & Baluška, F. (2006). The Root Apex of *Arabidopsis thaliana* Consists of Four Distinct Zones of Growth Activities: Meristematic Zone, Transition Zone, Fast Elongation Zone and Growth Terminating Zone. *Plant Signaling & Behavior*, *1*(6), 296–304. https://doi.org/10.4161/psb.1.6.3511

Ambrose, J. C., Shoji, T., Kotzer, A. M., Pighin, J. A., & Wasteneys, G. O. (2007). The Arabidopsis CLASP Gene Encodes a Microtubule-Associated Protein Involved in Cell Expansion and Division. *The Plant Cell*, *19*(9), 2763–2775. https://doi.org/10.1105/tpc.107.053777

Grieneisen, V. A., Xu, J., Marée, A. F. M., Hogeweg, P., & Scheres, B. (2007). Auxin transport is sufficient to generate a maximum and gradient guiding root growth. *Nature*, *449*(7165), 1008–1013. https://doi.org/10.1038/nature06215

Hamant, O., & Traas, J. (2010). The mechanics behind plant development. *New Phytologist*, *185*(2), 369–385. https://doi.org/10.1111/j.1469-8137.2009.03100.x

Ambrose, C., Allard, J. F., Cytrynbaum, E. N., & Wasteneys, G. O. (2011). A CLASP-modulated cell edge barrier mechanism drives cell-wide cortical microtubule organization in Arabidopsis. *Nature Communications*, *2*(1), 430. https://doi.org/10.1038/ncomms1444

van Esse, G. W., van Mourik, S., Stigter, H., ten Hove, C. A., Molenaar, J., & de Vries, S. C. (2012). A Mathematical Model for BRASSINOSTEROID INSENSITIVE1-Mediated Signaling in Root Growth and Hypocotyl Elongation. *Plant Physiology*, *160*(1), 523–532. https://doi.org/10.1104/pp.112.200105

Chaiwanon, J., & Wang, Z.-Y. (2015). Spatiotemporal Brassinosteroid Signaling and Antagonism with Auxin Pattern Stem Cell Dynamics in Arabidopsis Roots. *Current Biology*, *25*(8), 1031–1042. https://doi.org/10.1016/j.cub.2015.02.046

Kumpf, R. P., & Nowack, M. K. (2015). The root cap: A short story of life and death. *Journal of Experimental Botany*, *66*(19), 5651–5662. https://doi.org/10.1093/jxb/erv295

Vragović, K., Sela, A., Friedlander-Shani, L., Fridman, Y., Hacham, Y., Holland, N., Bartom, E., Mockler, T. C., & Savaldi-Goldstein, S. (2015). Translatome analyses capture of opposing tissue-specific brassinosteroid signals orchestrating root meristem differentiation. *Proceedings of the National Academy of Sciences*, *112*(3), 923–928. https://doi.org/10.1073/pnas.1417947112

Di Mambro, R., De Ruvo, M., Pacifici, E., Salvi, E., Sozzani, R., Benfey, P. N., Busch, W., Novak, O., Ljung, K., Di Paola, L., Marée, A. F. M., Costantino, P., Grieneisen, V. A., & Sabatini, S. (2017). Auxin minimum triggers the developmental switch from cell division to cell differentiation in the Arabidopsis root. *Proceedings of the National Academy of Sciences*, *114*(36), E7641–E7649. https://doi.org/10.1073/pnas.1705833114

Ruan, Y., Halat, L. S., Khan, D., Jancowski, S., Ambrose, C., Belmonte, M. F., & Wasteneys, G. O. (2018). The Microtubule-Associated Protein CLASP Sustains Cell Proliferation through a Brassinosteroid Signaling Negative Feedback Loop. *Current Biology*, *28*(17), 2718–2729.e5. https://doi.org/10.1016/j.cub.2018.06.048

Ackerman-Lavert, M., & Savaldi-Goldstein, S. (2020). Growth models from a brassinosteroid perspective. *Current Opinion in Plant Biology*, *53*, 90–97. https://doi.org/10.1016/j.pbi.2019.10.008

Salvi, E., Rutten, J. P., Mambro, R. D., Polverari, L., Licursi, V., Negri, R., Ioio, R. D., Sabatini, S., & Tusscher, K. T. (2020). A Self-Organized PLT/Auxin/ARR-B Network Controls the Dynamics of Root Zonation Development in Arabidopsis thaliana. *Developmental Cell*, *53*(4), 431–443.e23. https://doi.org/10.1016/j.devcel.2020.04.004

Matosevich, R., & Efroni, I. (2021). The quiescent center and root regeneration. *Journal of Experimental Botany*, *72*(19), 6739–6745. https://doi.org/10.1093/jxb/erab319

Vukašinović, N., Wang, Y., Vanhoutte, I., Fendrych, M., Guo, B., Kvasnica, M., Jiroutová, P., Oklestkova, J., Strnad, M., & Russinova, E. (2021). Local brassinosteroid biosynthesis enables optimal root growth. *Nature Plants*, *7*(5), 619–632. https://doi.org/10.1038/s41477-021-00917-x

Halat, L. S., Bali, B., & Wasteneys, G. (2022). Cytoplasmic Linker Protein-Associating Protein at the Nexus of Hormone Signaling, Microtubule Organization, and the Transition From Division to Differentiation in Primary Roots. *Frontiers in Plant Science*, *13*. https://doi.org/10.3389/fpls.2022.883363

Goh, T., Song, Y., Yonekura, T., Obushi, N., Den, Z., Imizu, K., Tomizawa, Y., Kondo, Y., Miyashima, S., Iwamoto, Y., Inami, M., Chen, Y.-W., & Nakajima, K. (2023). In-Depth Quantification of Cell Division and Elongation Dynamics at the Tip of Growing Arabidopsis Roots Using 4D Microscopy, AI-Assisted Image Processing and Data Sonification. *Plant and Cell Physiology*, *64*(11), 1262–1278. https://doi.org/10.1093/pcp/pcad105

Smithers, E. T., Luo, J., & Dyson, R. J. (2024). A continuum mechanics model of the plant cell wall reveals interplay between enzyme action and cell wall structure. *The European Physical Journal E*, *47*(1), 1. https://doi.org/10.1140/epje/s10189-023-00396-2